

Numerical Model of Fiber Orientation in the Converging Section of a Paper-machine Headbox using Large Eddy Simulation

Xiaosi Feng, Suqin Dong, Ian Gartshore and Martha Salcudean

Dept. of Mechanical Engineering, University of British Columbia,
2054-6250 Applied Science Lane, Vancouver, B.C., V6T 1Z4, Canada

ABSTRACT

The headbox is a critical component in the papermaking system. The rapidly converging section of a paper-machine headbox carries a dilute concentration of pulp fibers to the wire mesh where the fibers are dried to become paper.

A large eddy simulation (LES) is carried out to model the flow field in the converging section. A Lagrangian tracking scheme capable of simulating the motion of flexible or rigid individual fibers been devised and is coupled with the LES representation of turbulence in the converging section to predict the statistical orientation of nylon "fibers". The numerical results give statistical results which are similar to experimental data for the fiber orientation. The predicted orientation distributions with LES at the exit of the converging section are significantly better than those found using the $k-\varepsilon$ model for turbulence.

NOMENCLATURE

C_s	Smagorinsky constant
G	filter function
p	pressure
\mathbf{u}	velocity
u'	resolved rms fluctuation in streamwise direction
v'	resolved rms fluctuation in spanwise direction
w'	resolved rms fluctuation in normal wall direction
α	orientation angle
ρ	density
μ	dynamic viscosity
ν_T	eddy viscosity
χ_u	relaxation coefficient

1 INTRODUCTION

The headbox is the first component of a paper machine in the papermaking system. The fiber orientation and basis weight profiles of the paper depend on the fluid flow in the headbox, which makes a headbox critical to a successful papermaking system.

The headbox can be several meters wide in the cross machine direction and has a contraction ratio (inlet area to outlet area) of 10 or more in a streamwise length of less than a meter. A dilute concentration of pulp fibers in water flows steadily through the headbox. One of its functions is to provide a discharge of stock (fibers and other

substances in fluid suspension) at its outlet that is uniform in both the machine direction (MD) and across the width of the paper web (the cross direction). The stock is fed onto the forming section through a slice (exit of the headbox) opening.

To achieve good paper formation, there must be no fiber flocculation in the jet exiting the headbox. The fibers must also have an even distribution in the cross direction of the machine. Thus the flow in the headbox should have a minimal component of mean velocity in the cross-machine direction. At the same time, the maintenance of high intensity turbulence within the stock is required in headbox designs to prevent fiber flocculation. The turbulence that occurs in the converging section does not affect the mean flow distribution significantly but it is critically important because turbulence prevents unwanted fiber flocculation and provides a degree of dispersion for the fibers. A detailed understanding of this turbulence is therefore essential in order to study the fiber motion and to predict the quality of the paper produced.

Shimizu and Wada (1992) have calculated the flow of water in a generic headbox using the $k-\varepsilon$ model. They calculated the relationship between the varying height in the contracting part and the flow velocity distribution at the exit. The flow distribution was investigated in two dimensions and the jets from the diffuser tubes were modelled three-dimensionally. Hämäläinen (1993) used a finite element method to model the manifold, the turbulence generating section, and the slice in two dimensions. Aidun and Kovacs (1995) have focussed on the study of secondary flows in the headbox and their effects on non-uniform fiber orientation and mass. A non-linear $k-\varepsilon$ model developed by Speziale (1987) was employed. They reported surprisingly large secondary flows at the headbox exit. Bandahakavi and Aidun (1999) investigated the turbulent flow in the converging section of a headbox using the RNG $k-\varepsilon$ model and the Reynolds Stress Model (RSM). The RNG $k-\varepsilon$ model is an improved version of the standard $k-\varepsilon$ model (Chowdhury 1993). They found that the results obtained from the RSM model are superior to those of the RNG $k-\varepsilon$ model. Parsheh and Dahlkild (1999) compared the results of representing the turbulence with different models. It was observed that the turbulence energy computed by the $k-\varepsilon$ linear model is exaggerated. He *et al.* (1998) and Hua *et al.* (1999, 2000) have done a complete modelling of the manifold along with all the individual tubes with the $k-\varepsilon$ model in three dimensions.

Shariati, *et al.* (2000, 2001) and Shariati (2002) studied the headbox flow both experimentally and numerically.

Fiber orientation, both in the plane of the paper and in the paper thickness direction, significantly affects the paper quality (Loewen 1997). Here, fiber orientation refers to the angular distribution of fibers relative to the paper-machine direction. Ullmar and Norman (1997) and Ullmar (1998) investigated experimentally the effect of the headbox contraction ratio on fiber orientation. They found that the effect of the contraction ratio is more significant on fiber orientation than that of the flow rate. The fibers have been found to be more strongly orientated in the machine direction for higher contraction ratios. Zhang (2001) measured the fiber orientations along the centreline of an asymmetric headbox. He also predicted the fiber orientation in both symmetric and asymmetric headboxes using a fiber model, but only using the mean flow field obtained from the $\kappa - \varepsilon$ model. His comparison between the measured and predicted results showed that the simulated orientations tend to align more with the flow than the experimentally observed results because the turbulence was not taken into consideration for his calculation. Olson (2002) provided an analytic expression for the fiber orientation distribution in a headbox flow, neglecting the effect of turbulent dispersion. Olson *et al.* (2004) proposed an Eulerian model of a turbulent fiber suspension through a one-dimensional headbox to predict the fiber orientation distribution. Dong *et al.* (2002) partially considered the turbulence effect with a single fixed velocity field found through LES simulation. In this paper, the fiber calculation executes one step after which the flow is updated with LES. This means the flow distribution for fibers is changed at each time step to consider more realistic turbulence effects in the simulation.

2 MODEL DESCRIPTION

2.1 LARGE EDDY SIMULATION

The incompressible Navier-Stokes equations for constant viscosity ν can be written in the following form

$$\frac{\partial u_i}{\partial x_i} = 0 \quad (1)$$

$$\frac{\partial u_i}{\partial t} + \frac{\partial u_i u_j}{\partial x_j} = -\frac{1}{\rho} \frac{\partial p}{\partial x_i} + \nu \frac{\partial^2 u_i}{\partial x_j \partial x_j} \quad (2)$$

where the indices $i, j = 1, 2, 3$ refer to x, y and z .

Einstein's summation convention is applied, and u_i is the velocity in i -direction.

In LES, a filtering operation is performed on the Navier-Stokes equations to remove the small spatial scales. The resulting equations that describe the space-time evolution of the "large eddies" contain the subgrid scale stress tensor that describes the effect of the unresolved small scales on the resolved larger scales. The filtering procedure is applied to the flow-field variables according to

$$\bar{\phi}(x, \Delta, t) = \int_D G(x - x^*, \Delta, t) \phi(x^*, t) d^3 x^*,$$

where Δ is filter width, G is a filter function with property:

$$\int_D G(x - x^*, \Delta, t) d^3 x^* = 1.$$

A finite volume discretization involves a box-filter with

$$G(|x - \xi|, \Delta) = \begin{cases} \frac{1}{\Delta x_1 \Delta x_2 \Delta x_3} & |x_i - \xi_i| < \Delta x_i / 2 \\ 0 & \text{otherwise} \end{cases} \quad i = 1, 2, 3.$$

After applying the above box-filter to equations (1) and (2), we can get the filtered Navier-Stokes equations:

$$\frac{\partial \bar{u}_i}{\partial x_i} = 0 \quad (3)$$

$$\frac{\partial \bar{u}_i}{\partial t} + \frac{\partial \bar{u}_i \bar{u}_j}{\partial x_j} = -\frac{1}{\rho} \frac{\partial \bar{p}}{\partial x_i} + \nu \frac{\partial^2 \bar{u}_i}{\partial x_j \partial x_j} - \frac{\partial \tau_{ij}}{\partial x_j} \quad (4)$$

where the subgrid-scale (SGS) Reynolds stress tensor is written as

$$\tau_{ij} = \overline{u_i u_j} - \bar{u}_i \bar{u}_j \quad (5)$$

In order to solve the equations (3) and (4), the SGS Reynolds stress must be represented with a subgrid scale model.

2.1.1 SUBGRID MODEL

The most commonly used SGS model is the Smagorinsky model (1963). The model assumes the SGS stress follows a gradient-diffusion process, similar to molecular motion. Consequently, τ_{ij} is given by

$$\tau_{ij} - \frac{1}{3} \tau_{kk} \delta_{ij} = -2C_s \Delta^2 |\bar{S}| \bar{S}_{ij} = -2\nu_T \bar{S}_{ij} \quad (6)$$

where ν_T is the eddy viscosity related only to the smaller

scale motions, $\bar{S}_{ij} = \frac{1}{2} \left(\frac{\partial \bar{u}_i}{\partial x_j} + \frac{\partial \bar{u}_j}{\partial x_i} \right)$ is the filtered rate of

strain tensor, $|\bar{S}| = \sqrt{2\bar{S}_{ij}\bar{S}_{ij}}$ is the magnitude of the strain

tensor and C_s is the Smagorinsky constant ($0.1 \leq C_s \leq 0.24$, Rogallo and Moin (1984)). Here

$\Delta = (\Delta x_1 * \Delta x_2 * \Delta x_3)^{\frac{1}{3}}$ is the filter width, $\Delta x_i (i = 1, 2, 3)$ is i -direction grid spacing. In the region close to the wall, the eddy viscosity has to be reduced, which is usually achieved by using a Driest damping function:

$$\nu_T = -C_s [(1 - e^{-y^+/25}) \Delta]^2 |\bar{S}| \quad (7)$$

Several alternative models for the subgrid scale turbulence have been proposed: Yakhot *et al.* (1989) proposed a subgrid-scale model based on renormalization group (RNG) theory for the study of channel flow. Lesieur and Metais (1996) showed that Kraichnan's spectral eddy viscosity can be implemented in physical space, yielding the so-called structure-function model.

A more flexible model for the subgrid turbulence has been devised by Germano *et al.* (1991), the Dynamic SGS model. Their formulation begins with the Smagorinsky eddy-viscosity approximation. However, rather a fixed value of C_s a priori, they permit it to be computed as the LES proceeds.

For the finite volume method, a box-filter is considered for 'implicit' filtering of the Navier-Stokes equations. This approach has the advantage that it does not need to define a filter function. There are no explicit filter operations.

In contrast, a filter is defined when explicit filtering is used. The flow is divided into resolved and subfilter-scale (SFS) motions. The SFS motions can be further divided into resolved SFS (RSFS) and unresolved SFS (USFS) (Zhou *et al.* 2001, Carati *et al.* 2001). The USFS is commonly called SGS. The RSFS motions can be reconstructed from the resolved motions. The SGS (USFS) can not be represented directly and must be modeled.

Stolz *et al.* (2001) used u^* to approximate the unfiltered solution u . The approximate deconvolution u^* is computed by applying the deconvolution operator Q_N to the filter quantity \bar{u}

$$u^* = Q_N * \bar{u} \quad (8)$$

The operator Q_N is obtained by expanding the inverse of the filter G as an infinite series and truncating it at finite N . This leads to Q_N as an approximation of G^{-1} ,

$$Q_N = \sum_{i=0}^N (I - G)^i \approx G^{-1} \quad (9)$$

where I is the identity operator (Stolz *et al.* 1999). It is found that the deconvolution order $N = 5$ is sufficient for numerical test cases (Stolz *et al.* 2001). Using (9), u^* can be computed by repeated filtering of \bar{u} from

$$u^* = Q_N \bar{u} = \bar{u} + (\bar{u} - \bar{\bar{u}}) + (\bar{u} - 2\bar{\bar{u}} + \bar{\bar{\bar{u}}}) + \dots \quad (10)$$

The subgrid-scale Reynolds stress tensor τ_{ij} in (5) can be divided into two terms: SGS and RSFS

$$\tau_{ij} = \overline{(u_i u_j - u_i^* u_j^*)} + \overline{(u_i^* u_j^* - \bar{u}_i \bar{u}_j)} \quad (11)$$

SGS(USFS) RSFS
To model the transfer of energy to small scales, represented by $\overline{u_i u_j - u_i^* u_j^*}$, a relaxation term $\chi_u (I - Q_N * G) * \bar{u}$ is added for ADM model. The RSFS term in (11) is moved to the left side of the filtered Navier-Stokes equation (4). The equation (4) with ADM model can be written into

$$\frac{\partial \bar{u}_i}{\partial t} + \frac{\partial \bar{u}_i u_j^*}{\partial x_j} = -\frac{1}{\rho} \frac{\partial \bar{p}}{\partial x_i} + \nu \frac{\partial^2 \bar{u}_i}{\partial x_j \partial x_j} - \chi_u (I - Q_N * G) * \bar{u}_i \quad (12)$$

Where $\chi_u > 0$ is a relaxation coefficient.

The relaxation coefficient χ_u can be determined dynamically (Stolz *et al.* 2001).

2.1.2 NUMERICAL METHODS

The governing equations (3), (4) (or (12)) are discretized by finite volumes using a staggered mesh system. The scheme used in this paper is based on a fraction-step method (Chorin 1968, Kim and Moin 1987). The pressure gradient and the incompressibility constraint are integrated implicitly in time. The convective and diffusive terms are treated explicitly with the second-order Adams-Bashforth scheme in time. For finite volume discretization, the flux is computed by a second-order accurate averaging which is therefore equivalent to second-order central difference scheme. The Poisson-like pressure equation is solved to satisfy the mass continuity. The fast Fourier transform is applied in the direction of periodicity, and the Bi-Conjugate Gradient Stabilized (Bi-CGSTAB Van den Vorst 1992) is then used to solve the 2D Poisson equation. Parallel computing is used for the

LES. The domain is decomposed in one direction and the data is distributed into multiprocessors. The communication occurs only at block boundaries. MPI (Message Passing Interface) is used to exchange the data among the processors. The implementation of these methods is described in more detail in Feng (2005).

2.2 FIBER MODEL AND WALL MODEL

The first investigation of the motion of a rigid, neutrally buoyant, ellipsoidal particle in a Stokes flow was conducted by Jeffery (1922). The Jeffery theory could be used to describe the motion of rigid fibers (Anczurowski and Mason 1967). However, pulp fibers have high aspect ratios and can have considerable flexibility and cannot be modelled well by Jeffery's theory (Mason 1954). A flexible fiber model based on Euler-Bernoulli beam bending theory was introduced by Lawryshyn (1996). The immersed boundary method was used in Stockie and Green (1998) to simulate the motion of flexible pulp fibers. Their work was restricted to two-dimensional simulations. A flexible fiber model was proposed in Ross and Klingenberg (1997). It was further developed by Dong (2002) to account for fiber-wall interaction. In this model, each fiber consists of N rigid spheroids connected through $N-1$ joints (see Figure 1). The fiber can bend and twist much like a real fiber because of the rotational freedom in each joint. The motion of the fiber is determined by solving each spheroid's translation and rotation equations that are derived from Newton's second Law and the law of the moment of momentum.

Fibers frequently touch the wall in pulp and paper equipment, so that a wall model that can efficiently deal with the fiber-wall interaction is needed. For a smooth wall, a two-dimensional wall model was developed by Olson (1996). The idea is that a reaction force normal to the wall is exerted on the fiber to stop the fiber passing through the solid wall, and the friction force tangential to the wall is proportional to the normal force on the fiber. Dong (2002, Dong *et al.* 2003) extended Olson's model to a three-dimensional universal wall model, which can deal with the fiber interaction in any wall geometry. The fiber model and the wall model developed by Dong (2002) will be used in the following simulations.

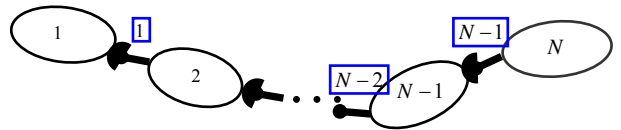


Figure 1 A fiber consisting of spheroids connected through ball and socket joints (from Ross and Klingenberg (1997)).

3 RESULTS

3.1 FLOW CALCULATION

Shariati (2002) has studied the flow in the converging section of a headbox both experimentally and numerically. The experimental headbox that he used is a laboratory scale model of a typical headbox with the size reduced by a factor of 5. The experimental set-up used a closed flow system, diagrammatically shown in Figure 2. In the flow loop, the water is pumped from the reservoir tank to the

headbox through the pipes and rectifier tubes. The rectifier tubes (or diffusers) are round at the inlet and rectangular at the outlet with slowly increasing cross sectional areas. They are used to provide turbulence energy for the flow and to generate a fairly uniform velocity profile at the converging section inlet. In Shariati's headbox model, there are 40 rectifier tubes, two rows in the vertical or height direction and 20 each in the spanwise or horizontal direction. The headbox section starts with a rectangular channel, which remains constant in cross section area until the length reaches 0.075 m. By means of LDV, Shariati (2002) measured the mean velocity and the rms velocity along the centreline of the converging section.

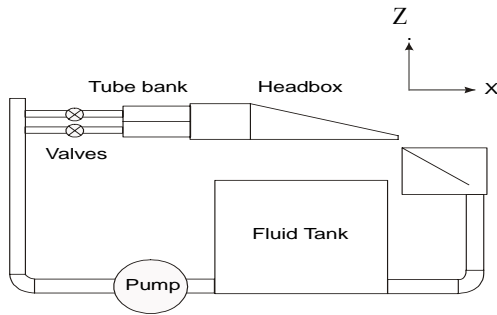


Figure 2 Flow loop in the experiment (from Shariati 2002).

The computational domain is shown in Figure 3. In the Z direction, no-slip wall boundary conditions are imposed along the solid walls. The spanwise direction, y , is treated as periodic.

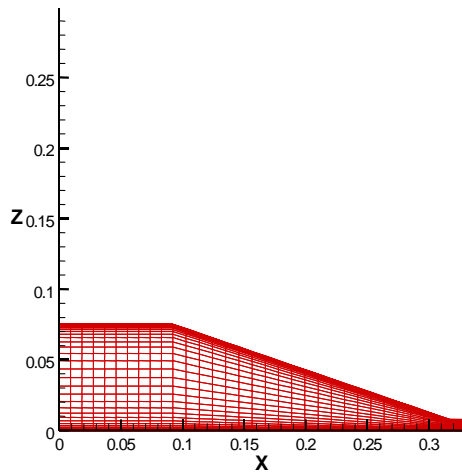


Figure 3 Computational domain for the converging section. Only a subset of the actual grid is plotted.

At the inlet plane the unsteady distributions for the velocity components generated by a separate LES of the fully developed channel flow that is modified with an extracting/rescaling technique (Lund *et al.* 1998) to match the measured inflow velocity fluctuation are specified.

The rescaling value is a common factor, the ratio of the computational rms velocity fluctuation u' and the experimental value at the centreline of the converging section. Different inflow conditions (for example a single, or alternatively a "two-channel" inflow condition) that simulate the turbulence produced by the rectifier tubes are discussed by Feng (2005). At the exit plane, the convective boundary condition (Kaltenbach 1998, Kaltenbach *et al.* 1999)

$$\frac{\partial u_i}{\partial t} + U_c \frac{\partial u_i}{\partial x} = 0 \quad (13)$$

is employed. U_c is set to the mean streamwise velocity at the exit plane. The dimensions of the computational domains are the same as the dimensions of the experimental apparatus except for the width in the spanwise direction. The computational domain spanwise width is approximately three inlet heights. A $64 \times 64 \times 64$ mesh is used. The meshes are uniform in the streamwise direction and in the spanwise direction. A non-uniform grid is used in the normal wall direction to resolve the near wall region.

The mean streamwise velocity along the centreline of the converging section is shown in Figure 4 using the constant Smagorinsky model. Here $X^* = x/L_x$ is the x position normalized with the total length of the converging section L_x . The computed value of the mean velocity agrees reasonably well with the measured value. The resolved rms fluctuations u', v' and w' normalized by u' at the inlet (u'_in) are presented in Figures 5–7. The rms fluctuation of the velocity in the X direction, u' diminishes towards the exit, while w' increases in the Z direction. The trend of the calculated results is the same as that of the experimental results, but there are some differences between them, particularly in the region between the inlet of the converging section and the first third of the converging section. This can be attributed to the difference between the measured and assumed inflow conditions. From the experiment, the two rows of tubes can generate much higher turbulence than the modified channel which is used as the model in the above calculations. The turbulence kinetic energy k nondimensionalized by k at the inlet of the position 0.006m after the convergence starts is shown in Figure 8. The turbulent kinetic energy predicted by LES and the standard $k-\varepsilon$ model in most of regions is close to the measured values. But the computed values with standard $k-\varepsilon$ model increase rapidly towards the exit. The reason is that the $k-\varepsilon$ model fails to predict the turbulence kinetic energy where the turbulence is significantly anisotropic at the exit of the converging section. Also, the standard $k-\varepsilon$ model includes a turbulence generation term that depends on $\partial U/\partial x$. That term becomes very large close to the exit of the converging section and causes a break down of the model (Shariati 2002).

The ADM model with the $64 \times 64 \times 64$ mesh is also carried out to consider the effect of the different subgrid models for the converging section. The comparison of mean streamwise velocity along the centreline of the converging section among the different subgrid models is shown in Figure 9. The comparisons of resolved rms fluctuations u' normalized by u' at the inlet (u'_in) among

the different subgrid coefficients is presented in Figures 10.

From the results, there is not much difference for two different subgrid models. The Smagorinsky constant $C_s = 0.1$ is therefore appropriate for the converging section coupling with a fiber model to predict the fiber orientation distributions in the next section.

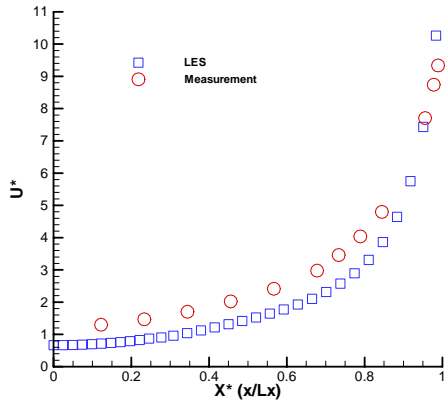


Figure 4 Comparison of the mean velocity at the centerline of the converging section.

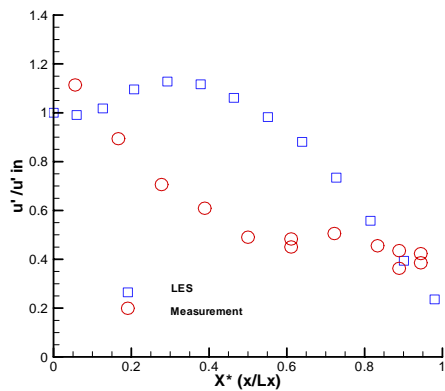


Figure 5 Comparison of rms value of the velocity fluctuation u' normalized by u'_{in} .

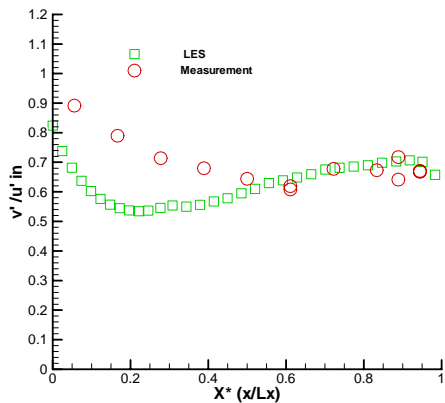


Figure 6 Comparison of rms value of the velocity fluctuation v' normalized by u'_{in} inlet condition.

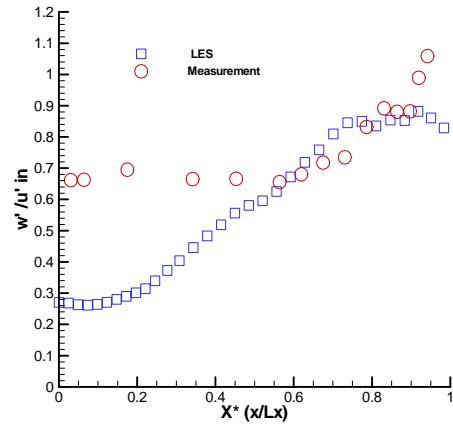


Figure 7 Comparison of rms value of the velocity fluctuation w' normalized by u'_{in} .

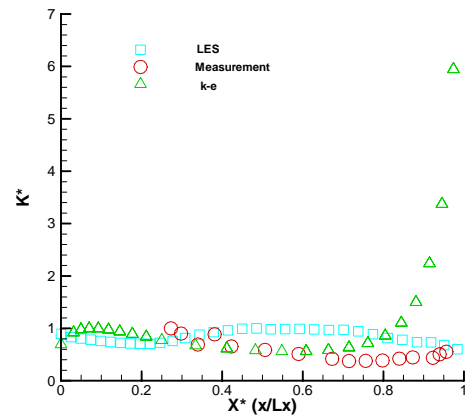


Figure 8 Comparison of turbulence kinetic energy k nondimensionalized by k at the inlet of the position 0.006m after the convergence starts.

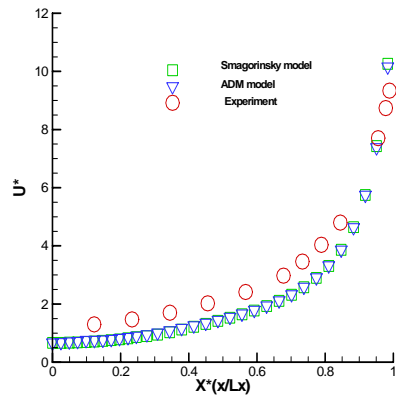


Figure 9 Comparison of the mean velocity at the centerline of the converging section with different subgrid models.

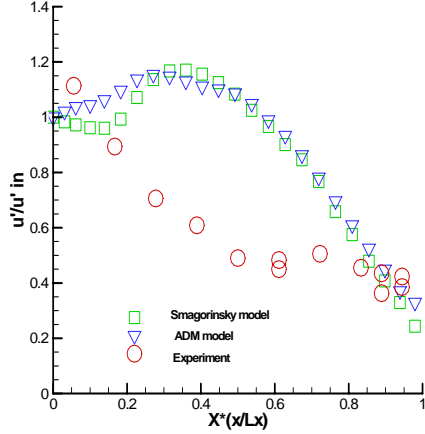


Figure 10 Comparison of rms value of the velocity fluctuation u' normalized by u'_{in} with different subgrid models.

3.2 FIBER ORIENTATION IN A HEADBOX

Fiber experiments have been conducted by Zhang (2001) to measure the orientation of dyed nylon fibers moving in a headbox model. The fibers have a nominal length of 0.003m and the diameter of 44 μm . The suspension is well within the dilute regime, with a consistency of no more than 0.001%, which means there is little interaction between fibers. In the experiment, video pictures were taken of fibers in motion at several locations along the center of the converging section.

3.2.1 INITIAL CONDITIONS

The fiber's position can be defined by three variables: fiber center (x_c, y_c, z_c) , polar angle $0 \leq \theta \leq \pi$, which is the angle between the fiber main axis and Z-axis, and the azimuthal angle $0 \leq \phi \leq \pi$, which is the angle between the Y-axis and the projection of the fiber main axis on XY plane (see Figure 11). It is noted that one end of the fiber is not distinguishable from the other.

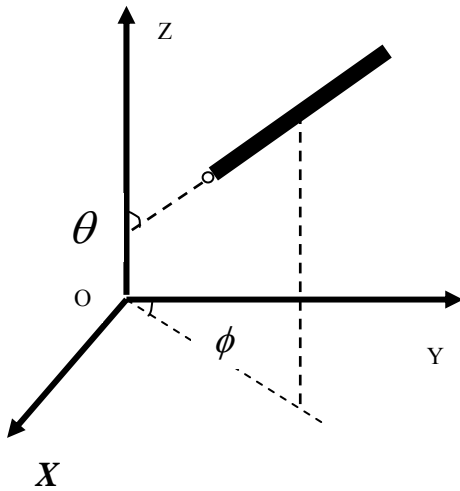


Figure 11 A fiber's initial position.

Eight thousand (8,000) rigid fibers of 0.003m length are initially chosen across 0.04 m region ($0.0175 m \leq z \leq 0.0575 m$) in the center of the inlet height with random location and random orientation. Random orientation is implemented by choosing the fiber angles θ and ϕ with random number generators. The angles θ and ϕ are not chosen randomly from uniform distributions $\theta \in [0, \pi]$ and $\phi \in [0, \pi]$, since the area element $d\Omega = \sin\theta d\phi d\theta$ is a function of θ on the surface of a unit sphere. So the angles are selected with the following formula (Zhang 2001):

$$\theta = \cos^{-1}(2a_1 - 1) \quad (14)$$

$$\phi = \pi a_2 \quad (15)$$

where a_1 and a_2 are random variables between $[0, 1]$.

3.2.2 NUMERICAL RESULTS

The projections of the orientation of fibers can be obtained in three different planes. The fiber orientation was only measured in both the plane of the paper (x-y) and in the plane of contraction (x-z) at the central streamline of the converging section along the axis of the headbox in Zhang (2001). The measurements were taken at several points along the headbox as shown in Figure 12. So the projections on two of the planes, x-y and x-z planes, are considered here. The fiber orientation angle

α ($-\frac{\pi}{2} \leq \alpha \leq \frac{\pi}{2}$), either on the x-y or on the x-z projection plane, is defined to be the angle between the projection of the fiber axis on that plane and the machine direction (x axis). Figures 13-14 show the initial fiber orientation distributions in the computation. The horizontal axis represents the orientation angle α . The vertical axis stands for the statistical probability density $p(\alpha)$, such that:

$$\int_{-\frac{\pi}{2}}^{\frac{\pi}{2}} p(\alpha) d\alpha = 1 \quad (16)$$

If the fiber orientation is uniform, then $p(\alpha) = 1/\pi$ (≈ 0.318). It can be seen that the initial random fiber orientation distribution is almost uniform from Figures 13-14. Figures 14-28 show the fiber orientation distributions at different stations. Most of the alignment occurs near the end of the converging section, beyond $x = 0.227m$, where the velocity gradient is the highest. The LES results predict the fiber orientation reasonably well when compared to the experimental data from Zhang (2001). From Figures 23-28, the $k-\varepsilon$ simulated fiber orientations tend to align more with the flow compared to experimental and LES results. At the exit where $x = 0.31m$, both $k-\varepsilon$ and LES predict that the fibers are highly aligned in the flow direction in x-z plane as shown in Figure 27. But the peak value of the distributions

using LES is lower than that using $k-\varepsilon$. Unfortunately there is no experimental data of fiber orientation at the exit in the $x-z$ plane, because the channel is too narrow and the flow speed is too high at that location to get clear fiber images (Zhang 2001). From the Figures 27-28, the fiber alignment in the $x-z$ plane is stronger than that in the $x-y$ plane. This phenomenon agrees with the observation in Zhang (2001) and Olson (2002).

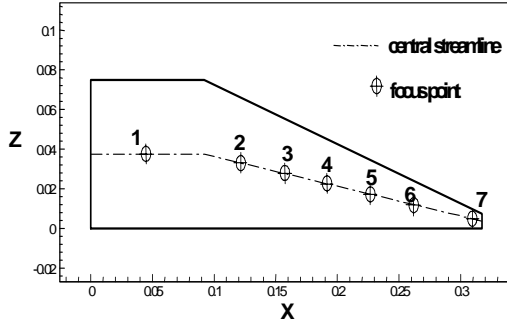


Figure 12 Measurement points along the headbox, unit m.

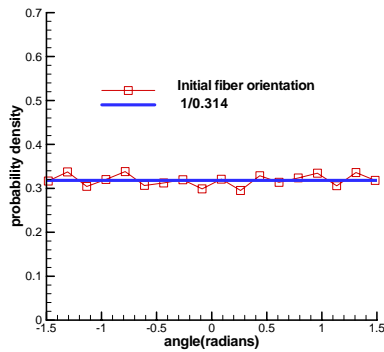


Figure 13 Initial fiber orientation distribution in x-z plane

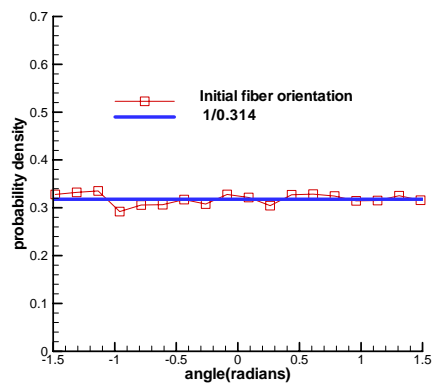


Figure 14 Initial fiber orientation distribution in x-y plane

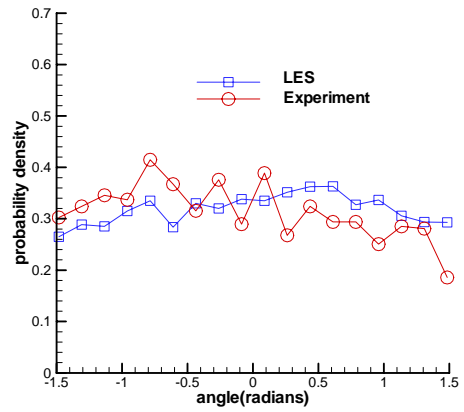


Figure 15 Fiber orientation distribution at $x = 0.045\text{m}$ in x-z plane

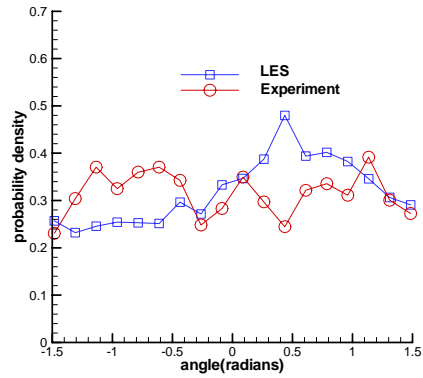


Figure 16 Fiber orientation distribution at $x = 0.045\text{m}$ in x-y plane

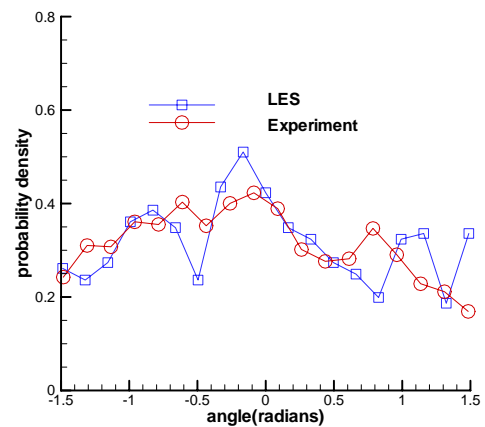


Figure 17 Fiber orientation distribution at $x = 0.122\text{m}$ in x-z plane

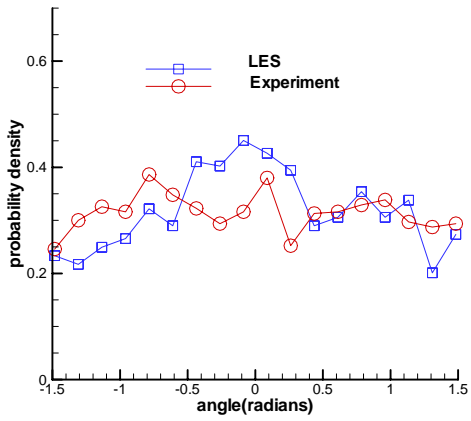


Figure 18 Fiber orientation distribution at $x = 0.122$ m in x-y plane

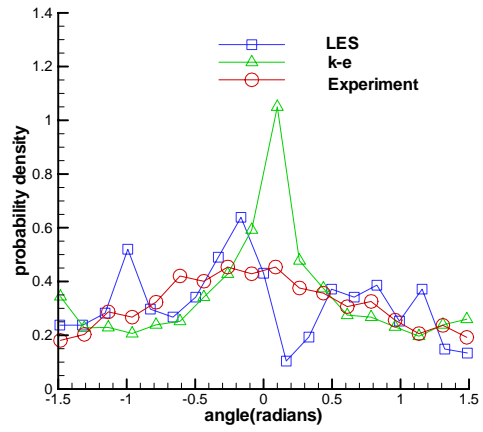


Figure 21 Fiber orientation distribution at $x = 0.192$ m in x-z plane

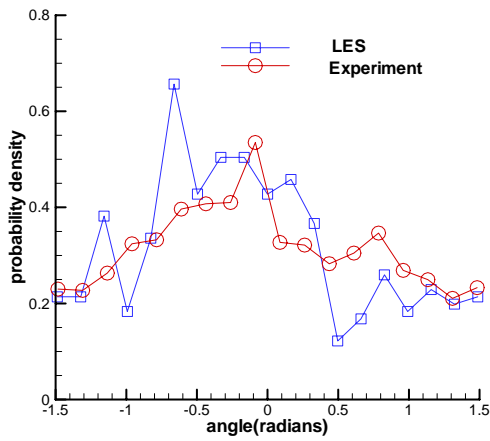


Figure 19 Fiber orientation distribution at $x = 0.157$ m in x-z plane

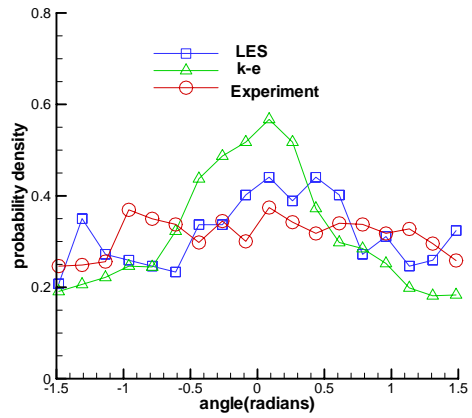


Figure 22 Fiber orientation distribution at $x = 0.192$ m in x-y plane

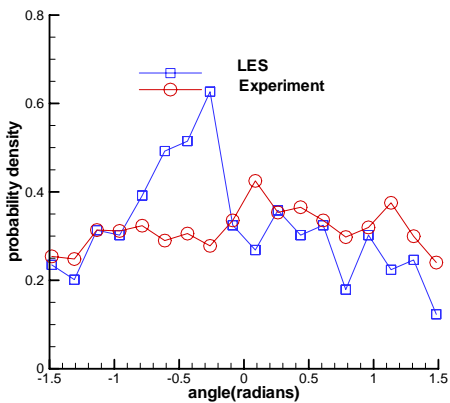


Figure 20 Fiber orientation distribution at $x = 0.157$ m in x-y plane

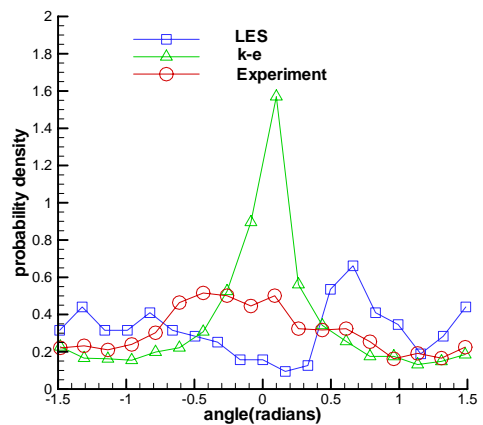


Figure 23 Fiber orientation distribution at $x = 0.227$ m in x-z plane

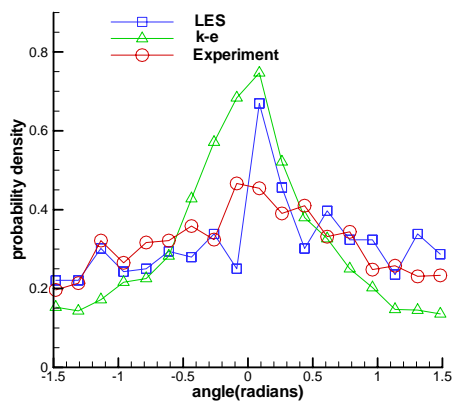


Figure 24 Fiber orientation distribution at $x = 0.227\text{m}$ in $x\text{-}y$ plane

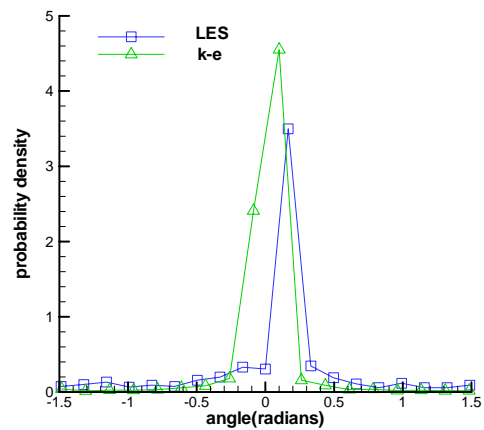


Figure 27 Fiber orientation distribution at the converging section exit in $x\text{-}z$ plane

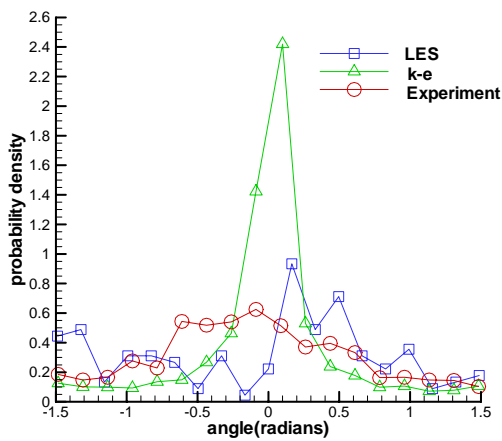


Figure 25 Fiber orientation distribution at $x = 0.262\text{m}$ in $x\text{-}z$ plane

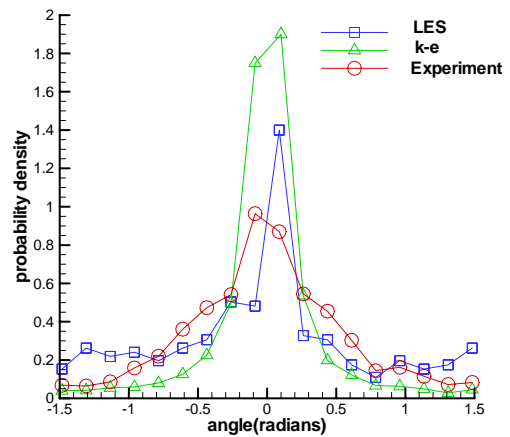


Figure 28 Fiber orientation distribution at the converging section exit in $x\text{-}y$ plane

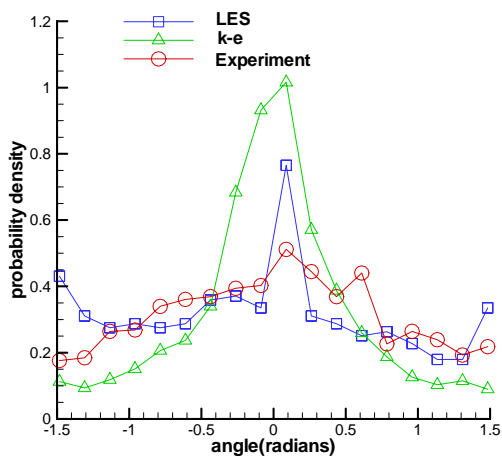


Figure 26 Fiber orientation distribution at $x = 0.262\text{m}$ in $x\text{-}y$ plane

4 CONCLUSION

The LES method has been used to simulate the turbulent flow through an asymmetric converging section. An important feature of this type of flow is that the turbulence is extremely non-isotropic near the exit when the contraction ratio is 10 or more. The standard $k-\varepsilon$ model spectacularly fails to predict the kinetic energy in this region.

The computed values of the mean velocity agree reasonably well with the measured values. For rms fluctuations, the trend of the calculation results is the same as that of the experimental results, but there are some differences between the numerical results and the measured results over the first third of the converging section length. This is probably caused by the difference in the inlet boundary conditions.

The LES and a fiber motion model have been coupled for predicting the orientation of rigid fibers in dilute suspensions. The effects of turbulence that would tend to randomize the fibers are observed in these simulations of

fiber motion. Random initial fiber orientations are set at the inlet of the channel. The statistical expressions of the orientation of a large number of fibers are evaluated at each station by computing the orientation of each single fiber along the central streamline. The LES results predict the fiber orientation reasonably well when compared to the experimental data. The predicted orientation distributions with LES are better than the $k - \varepsilon$ simulated fiber orientations near the exit of the converging section. The numerical results show that the LES calculation scheme can provide a useful method for the simulation of the interaction between fibers and complex fluid flow patterns.

REFERENCES

- Aidun, C. and Kovacs, A.E., (1995), "Hydrodynamics of the forming section: the origin of non-uniform fiber orientation", *TAPPI Journal*, 78(11), pp. 97-106.
- Anczurovski, E. and Mason, S.G., (1967), "The kinetics of flowing dispersions. II. Equilibrium orientations of rods and discs (experimental)", *J. Colloid Interface Sci.* 23, pp.533-546.
- Banhakavi, V. S. and Aidun, C. (1999), "Analysis of turbulent flow in the converging zone of a headbox", *TAPPI Engineering/Process and Product Quality Conference & Trade Fair*, pp.1135-1154.
- Carati, D., Winckelmans, G. and Jeanmart, H., (2001), "On the modelling of the subgrid-scale and filtered-scale stress tensors in large-eddy simulation", *J. Fluid Mech.* 441, pp.119-138.
- Chorin, A.J., (1968), "Numerical solution of the Navier-Stokes equations", *Math. Comput.*, 23, pp. 341-354.
- Chowdhury, D., (1993), "Introduction to the Renormalization Group method and turbulence modeling", Fluent Inc., TM-107 (cross-reference).
- Feng, X., (2005), "Large eddy simulation of the turbulence and fiber motion in a headbox", Ph.D. thesis, University of British Columbia.
- Dong, S., (2002), "Modeling of Fiber motion in pulp and paper equipment", Ph.D. thesis, University of British Columbia.
- Dong, S., Feng, X., Salcudean M. and Gartshore, I., (2003), "Concentration of pulp fibers in 3D turbulent channel flow", *Inter. J. Multiphase Flow*, vol. 29, 1, pp.1-21.
- Dong, S., Feng, X., Salcudean, M., Gartshore, I. and Shariati, M., (2002), "Turbulence and Fiber Orientation in the Converging Section of a Paper-machine Headbox", The 4th ASME/JSME/KSME Symposium on Computational Techniques for Fluid/Thermal/Chemical Systems with Industrial Applications, Vancouver, Canada.
- Germano, M., Poimelli, U., Cabot, W.H., and Moin, P., (1991), "A dynamic subgrid scale eddy viscosity model", *Phys. Fluids A*, 3(7), pp.1760-1765.
- Hämäläinen, J., (1993), "Mathematical modelling and simulation of fluid flows in the headbox of paper machines." Ph.D. Thesis, University of Jyväskylä.
- He, P., Bibeau, E. L., Hua, L., Salcudean, M. and Gartshore, I., (1998), "Fluid dynamics of the flow distribution in a headbox", CPPI conference, Montreal.
- Hua, L., Bibeau, E. L., He, P., Salcudean, M. and Gartshore, I., (1999), "Flow distribution in a hydraulic headbox." TAPPI Conference, Anaheim.
- Hua, L., He, P., Salcudean, M., Gartshore, I. and Bibeau, E. L., (2000), "Turbulent flow in hydraulic headbox", TAPPI conference, Vancouver.
- Jeffery, G. B., (1922), "The motion of ellipsoidal particles immersed in a viscous fluid", *Proc. Royal Soc.*, A102, pp.161-179.
- Kaltenbach, H., (1998), "Towards a near-wall model for LES of a separated diffuser flow". Annual Research Briefs, Center for Turbulence Research, NASA Ames/Stanford Univ., pp.255-265.
- Kaltenbach, H., Fatica, M., Mittal, R., Lund, T.S. and Moin, P., (1999), "Study of flow in a planar asymmetric diffuser using large-eddy simulations", *J. Fluid Mech.*, 390, pp. 151-185.
- Kim, J. and Moin, P., (1985), "Application of fractional-step method to incompressible Navier-stokes equations". *J. Comp. Phys.*, 59, pp.308-323.
- Lawryshyn, Y. A., (1997), "Statics and dynamics of pulp fibers", Ph.D. thesis, University of Toronto.
- Lesieur, M. and Metais, O., (1996), "New trends in large-eddy simulations of turbulence", *Annu. Rev. Fluid Mech.* 28, pp.45-82.
- Lund, T. S., Wu, X., and Squires, K. D., (1998), "generation of turbulent inflow data for spatially-developing boundary layer simulations", *J. Comp. Phys.*, 140, pp.233-258.
- Mason, S.G., (1954), "Fiber motions and flocculation", *TAPPI Journal*, 37(11), pp.494-501.
- Parsheh, M. and Dahlkild, A.A., (1999), "Modelling the flow around elastic guiding vanes and turbulence in a two-dimensional contraction", *TAPPI Engineering/Process and Product Quality Conference & Trade Fair*, pp.1433-1452.
- Olson, J. A., (1996), "The effect of fiber length on passage through narrow apertures", Ph.D. thesis, University of British Columbia.
- Olson, J. A., (2002), "Analytic estimate of the fiber orientation distribution in a headbox flow", *Nordic Pulp Paper Res. J.*, 17 (3), pp.302-306.
- Olson, J. A., Frigaard, I., Chan, C. and Hämäläinen, J., (2004), "Modeling a turbulent fibre suspension flowing in a planar contraction: The one-dimensional headbox", *Inter. J. Multiphase Flow*, vol. 30, 1, pp.51-66.
- Rogallo, R. S. and Moin, P., (1984), "Numerical simulation of turbulent flows". *Ann. Rev. Fluid Mech.* 16, pp.99-137.
- Ross, R. F. and Klingenberg, D. J., (1997), "Dynamic simulation of flexible fibers composed of linked rigid bodies", *J. Chem. Phys.* 106 (7), pp.2949-2960.
- Shariati, M. R., Bibeau, E., Salcudean M. and Gartshore, I., (2000), "Numerical and Experimental Models of Flow in the Converging Section of a Headbox", TAPPI Papermakers Conference, Vancouver, Canada.
- Shariati, M. R., Bibeau, E., Salcudean, M., Gartshore, I., Zhang, X. and Abdullah, Z., (2001), "Computational Investigation of the Flow through a Headbox", TAPPI Engineering and Finishing Conference, San Antonio.
- Shariati, M. R., (2002), "Experimental and mathematical modeling of flow in headboxes", Ph.D. thesis, the University of British Columbia.
- Shimizu, T. and Wada, K., (1992), "Computer simulation of measurement of flow in a headbox". *Proceedings of the Pan Pacific Pulp and Paper technology conference*, pp.157-165.

Smagorinsky, J., (1963), "General circulation experiments with the primitive equations". *Mon. Weather Rev.* 91(3), pp.99-164.

Speziale, C. G., (1987), "On nonlinear $k-l$ and $k-\epsilon$ models of turbulence", *J. Fluid Mech.*, 178, pp.459-475.

Stockie, J. M. and Green, S. I., (1998), "Simulating the motion of flexible pulp fibers using the immersed boundary method", *J. Comp. Phys.* 147, pp.147-165.

Stolz, S., and Adams, N.A., (1999), "An approximate deconvolution procedure for large-eddy simulation", *Phys. Fluids* 11, pp.1699-1701.

Stolz, S., Adams, N.A., and Kleiser, L., (2001), "An approximate deconvolution model for large-eddy simulation with application to incompressible wall-bounded flows", *Phys. Fluids* 13, pp.997-1015.

Ullmar, M. and Norman, B., (1997), "Observation of fiber orientation in a headbox nozzle at low consistency", TAPPI Proceedings, Engineering and Papermakers Conference, Anaheim, pp.865-869.

Ullmar, M., (1998), "On fiber orientation mechanisms in a headbox nozzle", Master's thesis, Royal Institute of Technology, Stockholm, Sweden.

Van der Vorst, H. A., (1992), "A fast and smoothly converging variant of BI-CG for the solution of nonsymmetric linear systems" *SIAM J. Sci. Statist. Comput.* 13, pp.631-644.

Yakhot, A., Orszag, S. A., Yakhot, V. and Israeli, M., (1989), "Renormalization group formulation of large-eddy simulations", *J. Sci. Comput.* 4, p.139.

Zhang, X., (2001), "Fiber orientation in Headbox", M. A. Sc thesis, University of British Columbia.

Zhou, Y, Brasseur, J. and Juneja, A., (2001), "A resolvable subfilter-scale model specific to large-eddy simulation of under-resolvable turbulence", *Phys. Fluids* 13, pp.2602-2610.

ACKNOWLEDGEMENT

The calculations are carried out in the PIII/Linux and P4-Xeon clusters at the University of British Columbia. We would like to acknowledge the financial assistance from FRBC and the Natural Science and Engineering Research Council of Canada (NSERC).